AMELIA[1] CESTOL[2] Test: Acoustic Characteristics of Circulation Control Wing and Leading- and Trailing-Edge Slot Blowing

William C. Horne[3] and Nathan J. Burnside[4]
NASA Ames Research Center, Moffett Field, CA 94035

Aeroacoustic measurements of the 11% scale full-span AMELIA CESTOL model with leading- and trailing-edge slot blowing circulation control (CCW) wing were obtained during a recent test in the Arnold Engineering Development Center 40- by 80-Ft. Wind Tunnel at NASA Ames Research Center. Sound levels and spectra were acquired with seven in-flow microphones and a 48-element phased microphone array for a variety of vehicle configurations, CCW slot flow rates, and forward speeds. Corrections to the measurements and processing are in progress, however the data from selected configurations presented in this report confirm good measurement quality and dynamic range over the test conditions. Array beamform maps at 40 kts tunnel speed show that the trailing edge flap source is dominant for most frequencies at flap angles of 0° and 60°. The overall sound level for the 60° flap was similar to the 0° flap for most slot blowing rates forward of 90° incidence, but was louder by up to 6 dB for downstream angles. At 100 kts, the in-flow microphone levels were louder than the sensor self-noise for the higher blowing rates, while passive and active background noise suppression methods for the microphone array revealed source levels as much as 20 dB lower than observed with the in-flow microphones.

Nomenclature

C_L	=	Lift coefficient, L / (q*S)
$C\mu$	=	CCW slow momentum coefficient, (m*V_j) / (q*S)
CCW	=	Circulation control wing
CSM	=	Cross-spectral matrix
L	=	Lift, lb_f
m	=	Slot mass flow rate, lb_m / s
OASPL	=	Overall sound pressure level, dB re 20^{-6} Pa
q	=	Freestream dynamic pressure, lb_f / ft^2
R	=	Radial distance from model acoustic center to sensor, inches
S	=	Wing planform reference area, ft^2
V_j	=	CCW slot jet velocity, ft / s
θ	=	Emission angle relative to model acoustic center, θ = 0° for upstream emission

I. Introduction

ACTIVE circulation control of lift has been considered to maintain lift at reduced flight speed for short takeoffs and landings, as well as to reduce the size and weight of control surfaces. The AMELIA CESTOL concept was a result of a collaboration between NASA, California Polytechnic University San Luis Obispo, and Georgia Tech Research Institute. The goal was to improve the ability to design and understand the performance of a modern aircraft with a leading- and trailing-edge circulation control wing and other features, such as above-wing propulsion to reduce community noise, as part of the NASA Fundamental Aeronautics program. The project culminated with a comparative assessment of CFD modeling of the complex vehicle aerodynamics with extensive aerodynamic and

[1] AMELIA – Advanced Model for Extreme Lift and Improved Aeroacoustics
[2] CESTOL – Cruise Efficient Short Take-Off and Landing
[3] Aerospace Engineer, Experimental Aero-Physics Branch, AIAA Associate Fellow.
[4] Aerospace Engineer, Experimental Aero-Physics Branch, AIAA Senior Member.

acoustic measurements of a sting-mounted, 11% scale-model in the Arnold Engineering Development Center 40- by 80-Foot Wind Tunnel at NASA Ames Research Center. Aerodynamic results from the test program are summarized by Jameson et al[1]. Some preliminary acoustic results were reported by Burnside and Horne[2], including representative measurements of propulsion simulator noise, comparisons of circulation control wing (CCW) noise spectra and overall levels for selected configurations, primarily for the 60° flap configuration.

The objectives of this paper are to describe acoustic measurements of the CCW system in more detail, to consider effects of parameters such as tunnel speed, CCW blowing rate, and flap angles of 0° and 60°, and to discuss plans for further data correction, processing, and reporting. This discussion will be based on model configurations for which the propulsion simulators and support pylons were removed and for an angle-of-attack of 0°.

II. Description of the Wind Tunnel Model

The AMELIA CESTOL model and test program were described by Jameson et al[3]. Development of the propulsion configuration and CCW design was described by Gaeta et al[4]. Figure 1 shows a cut-away drawing of the 10 ft (3.048 m) span model and blade support adaptor. High pressure air to drive the propulsion simulators was ducted through the support sting and blade attachment. Low pressure air for the CCW plenums was routed through two external hoses supplying air to distribution plenums in each wing. CCW air flow rate was metered externally with a digital valve, and supplied to the eight slots (inboard, outboard, leading- and trailing edge locations on each wing) through the wing ducting that was balanced with resistive elements prior to tunnel entry. Slot flow profiles at several spanwise stations were measured with a boundary-layer total pressure probe during the balancing exercise.

Figure 2 shows a cross section of the inboard wing at the 26% semi-span location with the 80° dual-radius flap

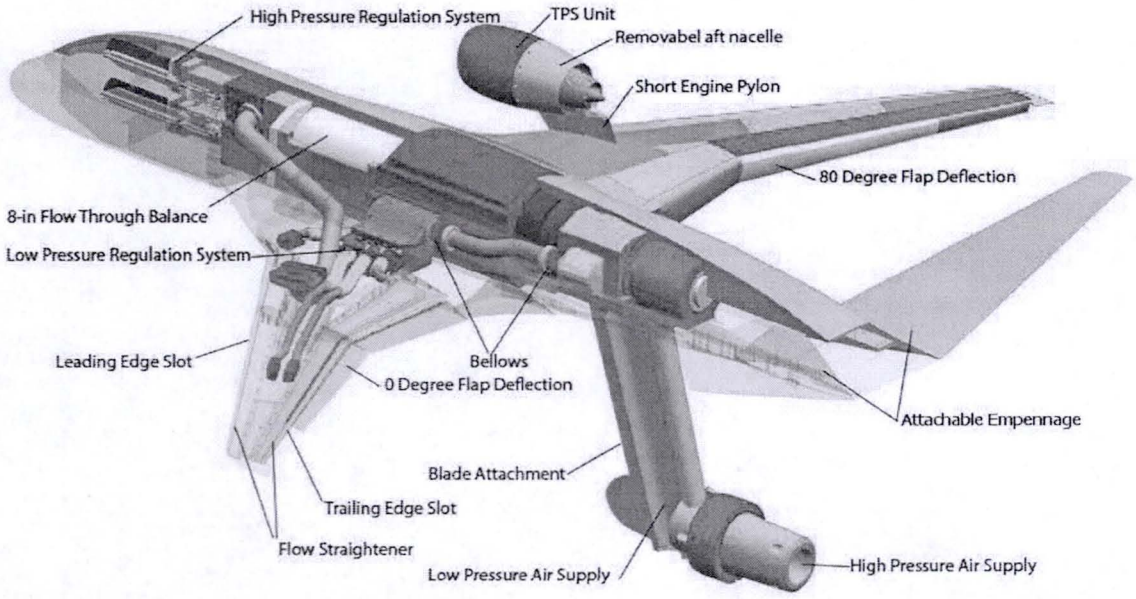

Figure 1. View of model internal components. TPS air is supplied through the sting / blade (high pressure air supply) CCW air from external hoses (low pressure air supply).

installed. Changes to the 0°, 30° and 60° flap configurations were accomplished by exchanging lower-wing/flap modules while maintaining constant slot height. For a flight configuration, the trailing-edge slots would be maintained at a fixed height by rotating the dual-radius flap about the axis of the smaller radius surface. Visible in this figure are the

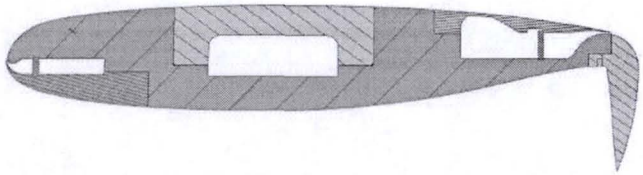

Figure 2. Inboard wing cross-section at 26% of semi-span from centerline (middle of inboard flap), flap angle 80°.

central plenum, leading- and trailing-edge plenums and the resistive-elements used for flow balancing.

The average heights were 0.025 in. (0.064 cm) for the leading edge slots (inboard and outboard), and 0.025 in. and 0.047 in. (0.12 cm) for the trailing-edge outboard and inboard slots, respectively. A table of the slot heights from Jameson[3] is reproduced in Table 1 located in the Appendix. The mass flow was divided approximately evenly between trailing- and leading-edge slots, however the trailing edge exit velocities were about 20% higher than for the leading edge, approaching sonic exit velocity at the highest flow rate.

III. Test Facility, Setup, and Instrumentation

The 11% full-span model was supported on a pitching sting mount attached to the turntable, providing yaw and pitch motion with a zero-pitch elevation above the floor of about 22 ft (6.71m) A description of the wind tunnel flow capabilities and acoustic treatment was provided by Burnside[2].

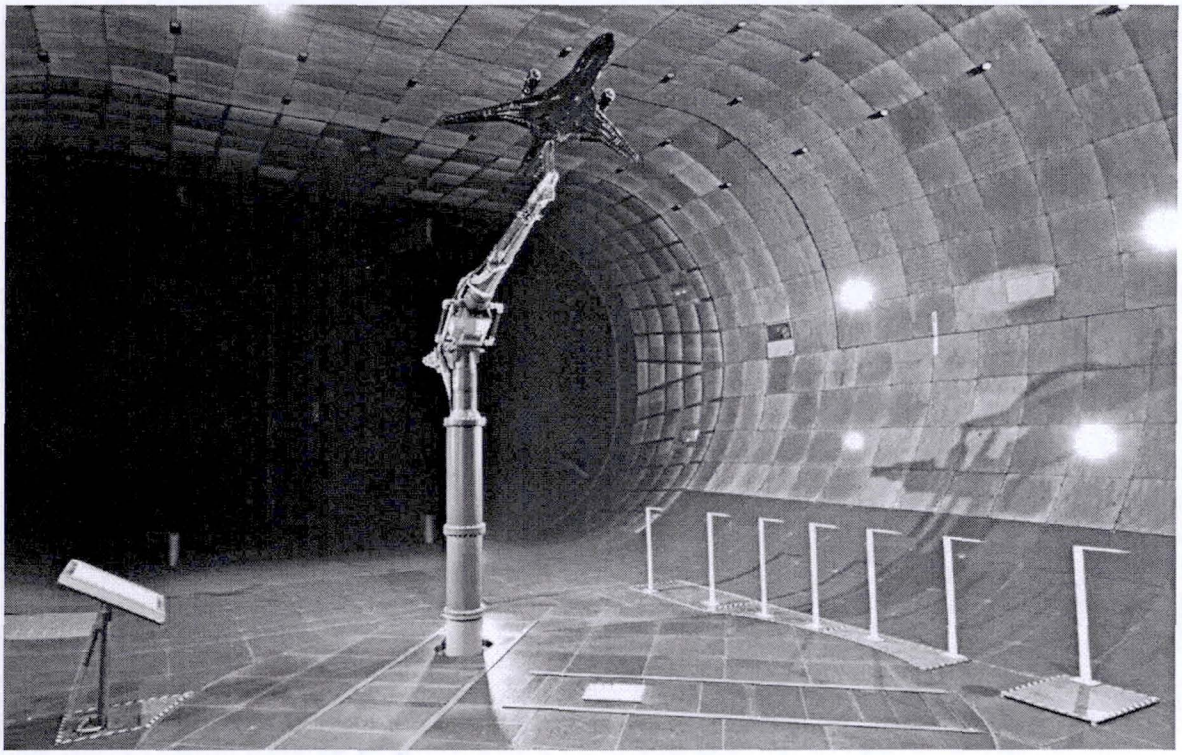

Figure 3. AMELIA CESTOL model mounted on pitching sting support in test section. Note array fairing *on model right, seven fixed microphones on the left.*

Figure 3 is a photograph of the model and acoustic sensors in the test section. A plan view of the acoustic sensor layout is provided in Fig. 4. Distances and angles from the model to the sensors are referenced to a model acoustic center, a point midway between the inboard/outboard break points in the wing trailing edge for a 0° flap deflection. For 0° angle-of-attack, distances and angles are given in Table 2. Note that microphone 6 and the phased array are located on the opposite sides of the model at approximately the same emission angles for 0° yaw.

The phased microphone array consisted of 48 G.R.A.S. ¼" 40BF free-field microphones and 26AC preamplifiers with diaphragms flush mounted on a 42.5 in. (1.08m) square aluminum plate recessed 0.5 in. (1.27 cm) behind 1.8 oz Kevlar cloth oriented parallel with the tunnel flow. The array plate was housed in an aerodynamic fairing 80 in. (2.03m) long by 50 in. (1.27m) wide, and rolled 30° from horizontal so that the array normal vector approximately intersected the model fuselage axis at 0° incidence and at 122° emission angle. The array pattern, (designed by Optinav, Inc) was approximately 40 in. (1.02 m) in diameter.

The seven individual microphones were also G.R.A.S. ¼" 40BF model with G.R.A.S. RA022 nosecones, and mounted on 72 in. high steel stands. Eight Kulite XCS-062 unsteady pressure sensors were placed on the left wing and fuselage side, as described by Burnside[2]. Acoustic and unsteady pressure signals were acquired at 96 kSamp/s with a 24-bit National Instruments PXI system, resulting in a usable bandwidth of 40 kHz model-scale, 4.4 kHz full-scale. Array signals were processed by the Optinav Beamform Interactive software, primarily using conventional beamforming and TIDY software, as described by Dougherty and Podboy[5]. MATLAB scripts developed by the coauthor provided data acquisition and automated processing of both array and microphone data.

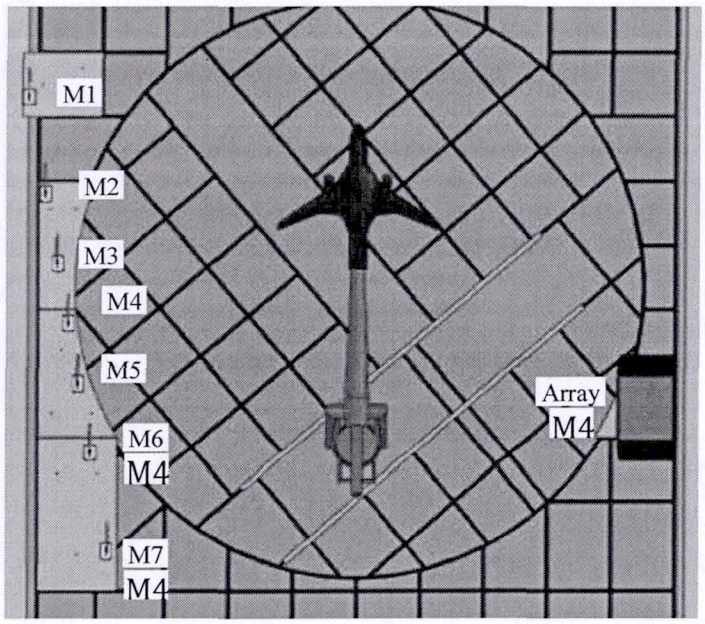

Figure 4. Planview of model and acoustic sensors in test section. Phased array on right side, fixed microphones on the left side.

Test data were acquired primarily at tunnel speeds of 40 kts (20.56 m/s, M = 0.06) and 100 kts (51.4 m/s, M = 0.15), but some data were acquired at additional speeds of 60, 80, and 120 kts. At 100 kts and maximum CCW air flow rate of 1.4 lb_m/sec (0.63 kg/s) per wing, the momentum coefficient, Cμ was 0.14, somewhat larger than typical active lift wing designs. At 40 kts with the same CCW flow rate, Cμ was 0.88. With the propulsion simulators removed, the CCW rate was swept in small increments from 0 to max for 40 and 100 kts, 0°, 60, and 80°flap, and 0° and 10° incidence. Some data was also acquired for similar settings with the leading edge slots blocked. The data presented here are uncorrected for directional sensor response since the corrections are being validated at this time. The correction magnitudes are estimated to be less than 3 dB below 10 kHz and less than 6 dB above 10 kHz for the array, and less than 2 dB below 10 kHz and less than 10 dB above 10 kHz for the fixed microphones.

IV. Results and Discussion

A. Near-field Acoustic Measurements of Isolated Right Wing

Prior to final model assembly and installation, the CCW flow ducting and slot heights on the right wing were balanced on a lab bench with resistive flow elements to generate as-designed exit velocities on the four right wing slots. The final configuration flow rate was calibrated with total pressure surveys at multiple stations on each slot. Following this task, the associated acoustic field from the wing at maximum CCW flow rate was sampled with an Optinav Array24Jr 24-element phased microphone array that had a microphone pattern diameter of about 15 in. (38.1 cm). The array was placed at 30° increments on a survey line about 4 ft (1.2 m) at approximately the same lateral angle of 45° as in the wind tunnel. Typical beamform maps at 60° and 120° flight path angles are shown in Fig. 5a and 5b., respectively. At the 60° angle, slot noise is radiated from both leading and trailing edge. At 120° only trailing edge noise is observed, showing that the leading edge slot noise is shielded by the wing. Spanwise variations in strength are visible for both leading- and trailing-edge sources, and may be due to a combination of effects of blowing rate, slot geometry, slot jet velocity at the trailing edge, and other factors.

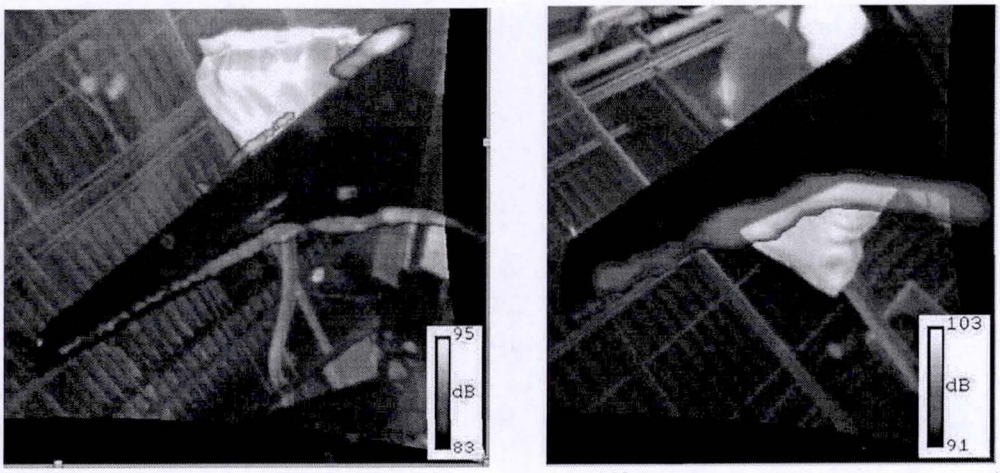

a) 60° b) 120°

Figure 5. Beamform maps from under isolated right-wing, with 1.4 lb_m/s leading-edge and trailing edge blowing, 0° flap, 8 kHz. Each image has a 12 dB range with an upper limit at the peak level for each image.

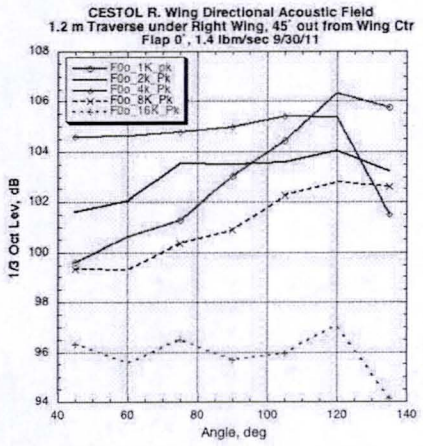

a) 0° flap

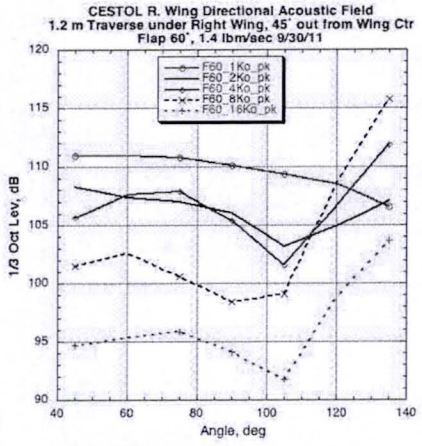

b) 60° flap

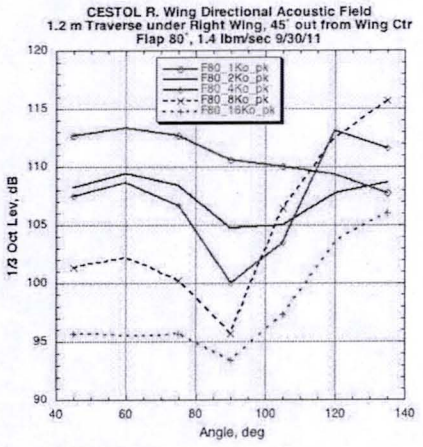

c) 80° flap

Figure 6. Spectra from beamform peak levels (TIDY) for all three flap angles.

Peak levels from the beamform maps were combined to estimate the directional radiation pattern from the wing for the 0°, 60°, and 80° flaps, as shown in Fig. 6. A relative minimum in the pattern is apparent for 60° and 80° flaps for frequencies above 1 kHz, consistent with baffled-dipole (cardioid shape) observed by Gaeta et al[6] for a 2-D wing section with similar CCW dual-radius flap geometry. Similar patterns have been observed for finite-length wall jets[7] as well as for airfoil trailing edge noise[8,9].

B. Wind Tunnel Measurements

In the wind tunnel, the microphone array and line of microphones were about 26 ft (8 m) from the model center, or about 7 times the measurement distance of the isolated wing described above. Wind tunnel measurements should be about 16 dB less than the near-field measurements discussed above. Wind-tunnel background noise also degrades signal-to-noise for the array and fixed microphones The microphone array proved useful in assessing relative strengths between the model CCW noise and other background sources such as the unfaired sting and sting support post. Figures 7 and 8 present beamform maps (TIDY process) of the model and forward sting in 1/3-octave bands centered at 1, 2, 4, 8, 16, and 32 kHz for the conditions of 40 kts tunnel speed, 0° flap (Fig. 7), and 60° flap (Fig. 8) . Sting noise is present at 1 kHz with a level comparable to the model noise for both flap angles. A source at the leading-edge root is present for frequencies 8 kHz and higher for the 0° flap, and at 32 kHz for the 60° flap, a feature not observed in the near-field measurement at the 120° emission angle corresponding to the wind-tunnel array. This is possibly noise emitted from the slot flow manifold inside of the wing.

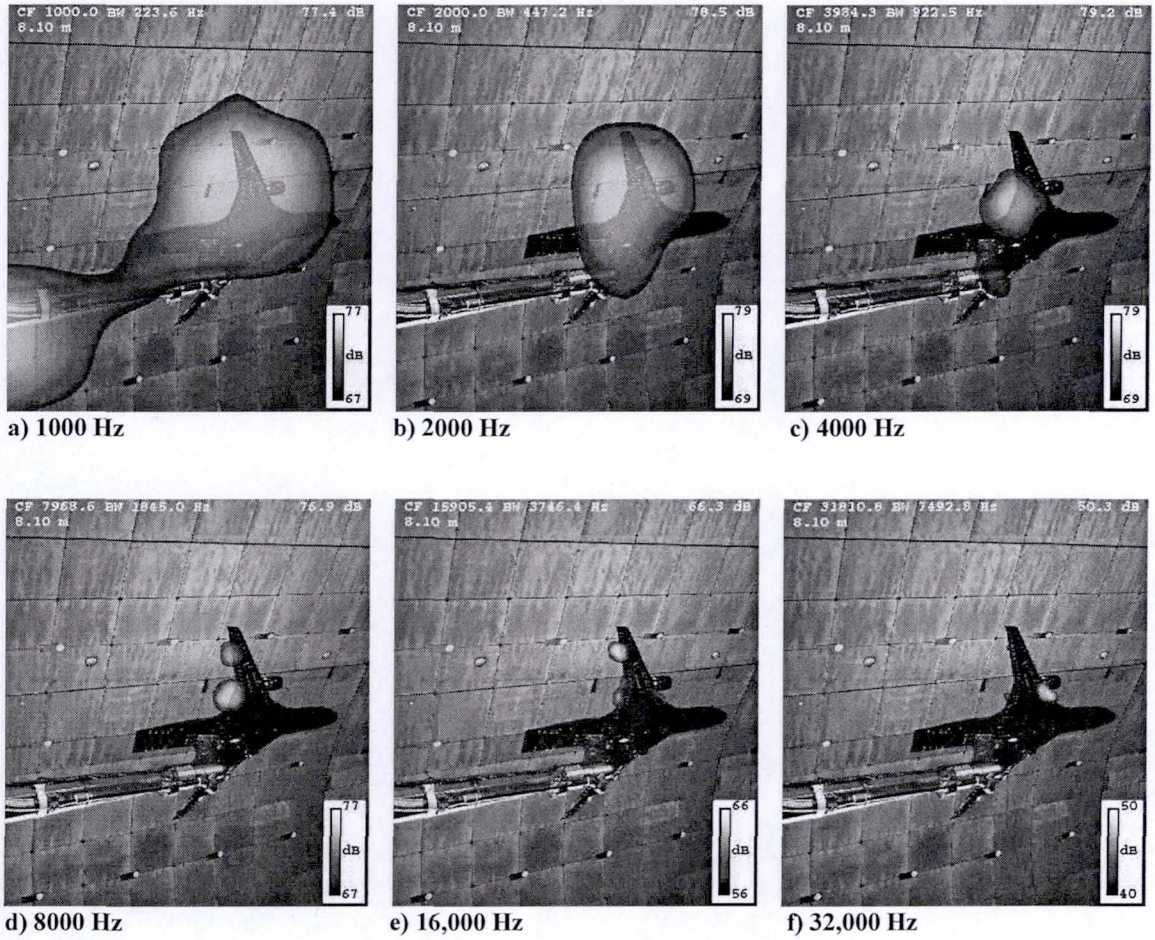

a) 1000 Hz b) 2000 Hz c) 4000 Hz

d) 8000 Hz e) 16,000 Hz f) 32,000 Hz

Figure 7. Array beamform maps (TIDY process), 1/3-octave center frequencies of 1, 2, 4, 8, 16, and 32 kHz model-scale or 110, 220, 440, 880, 1760, 3250 Hz full-scale. V = 40 kts, α = 0°, flap angle = 0°, max CCW ($C\mu$ = 0.88). The TPS units were removed for this condition, although visible in the photo used for beamform maps. Each image has a 10 dB range with an upper limit at the peak level for each image.

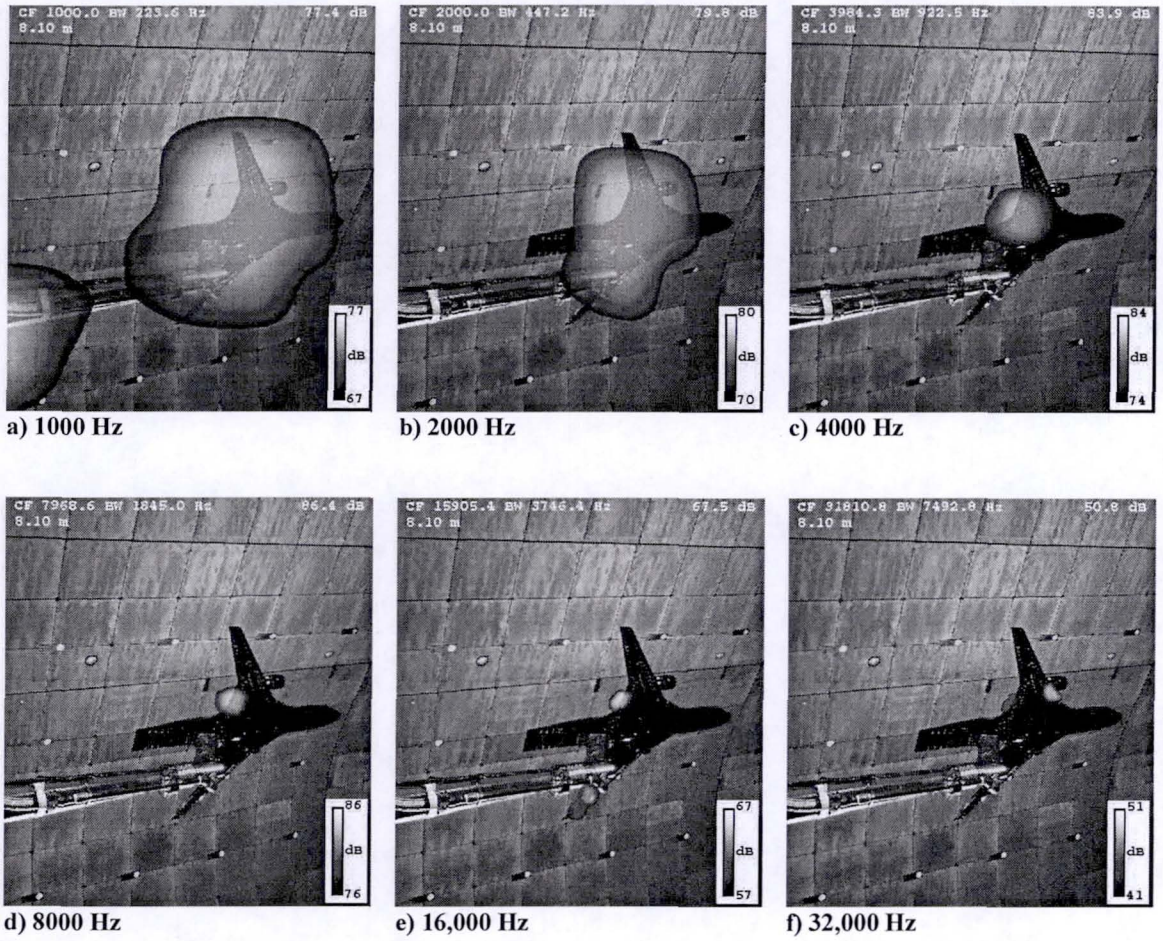

a) 1000 Hz **b) 2000 Hz** **c) 4000 Hz**

d) 8000 Hz **e) 16,000 Hz** **f) 32,000 Hz**

Figure 8. Array beamform maps (TIDY process), 1/3-octave center frequencies of 1, 2, 4, 8, 16, and 32 kHz model-scale or 110, 220, 440, 880, 1760, 3250 Hz full-scale. V = 40 kts, $\alpha = 0^o$, flap angle = 60^o, max CCW ($C\mu$ = 0.88). The TPS units were removed for this condition, although visble in the photo used for beamform maps. Each image has a 10 dB range with an upper limit at the peak level for each image.

At frequencies above 1 kHz the principal sources are seen along the wing at 2-32 kHz, although the distribution appears less uniform in the spanwise direction than in the near-field measurements from Fig 5. The distance from the array to the left and right wing tips varies by about 40% and the trailing-edge angles relative to the array vary across the wing. These varations could account for the nonuniformity in the beamform images. Slight differences between the source distributions for the two flap angles are seen along the trailing edge for frequencies above 1 kHz.

Figures 9a and 9b present trends of the 122° fixed microphone 1/3-octave spectra with Cμ variation for 40 kts, 0° α, for 0° and 60° flap respectively. Table 3 gives the overall blowing rates and corresponding Cμ values for 40 and 100 kts forward speeds. As Cμ increases from the lowest values for the 0° flap angle, the peak frequency and spectral levels increase rapidly. Above m = 0.5 lb_m/s, the spectra develop some tonal features in an otherwise broad shape. At 60° flap angle, the spectra trend to levels about 7 dB higher than the 0° case at higher values of Cμ, and a moderate peak at 6 kHz develops for the higher blowing rate.

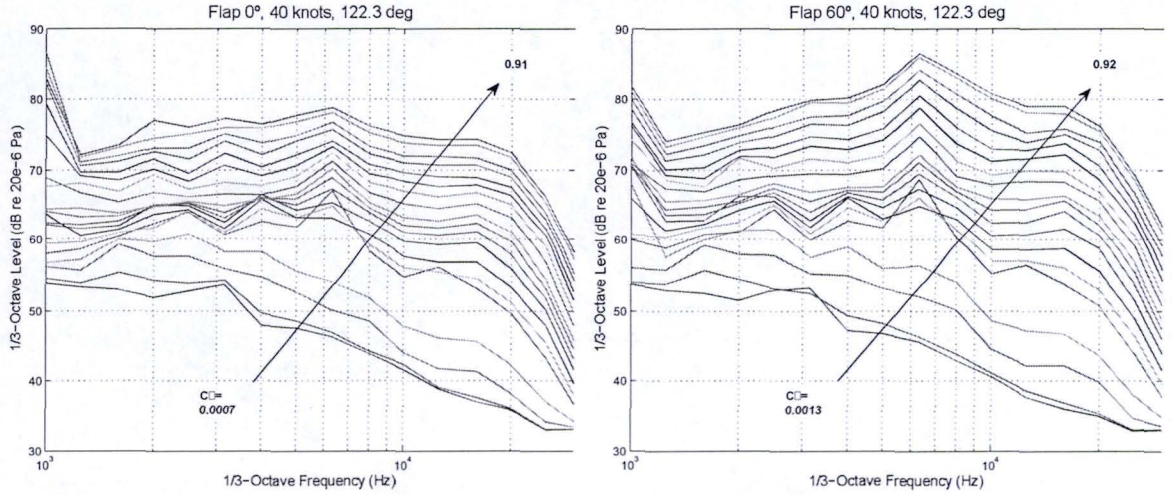

a) 0° flap **b) 60° flap**

Figure 9. Trend of 122° microphone 1/3-octave spectra with Cμ variation, V = 40 kts, α = 0°.

Figures 10a and 10b compare directional OASPL levels from the fixed microphones for conditions of 40 kts, 0° α, flap angle 0° and 60° respectively. The levels for the two flap settings are similar for emission angles of 90° and less. For emission angles higher than 90°, the 0° flap levels trend gradually downward, while the 60° levels continue to increase. For comparison, the directional levels of the TPS at the highest RPM are shown on the two figures, and exceed the max CCW curves by 5-10 dB.

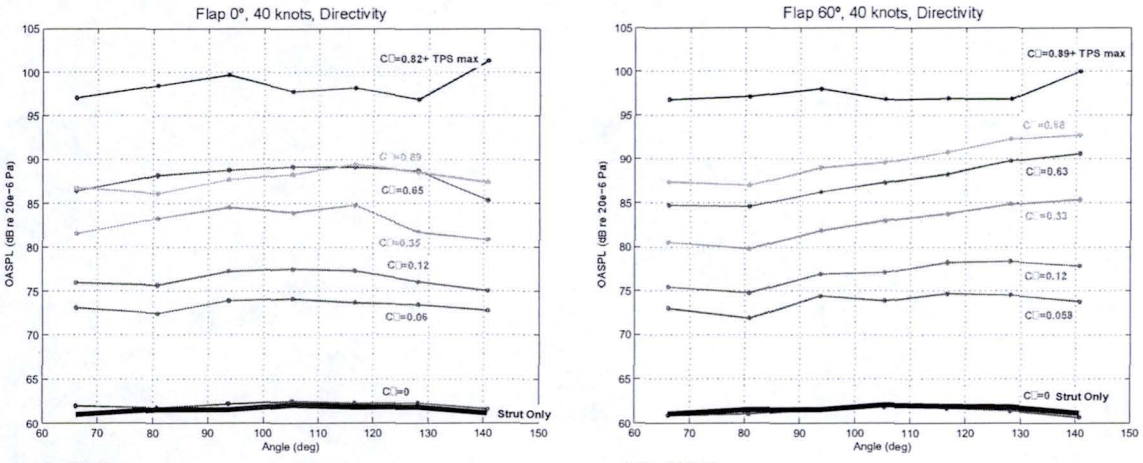

a) 0° flap **b) 60° flap**

Figure 10. Comparison of OASPL directional levels for selected Cμ, V = 40 kts, α = 0°. Highest level curve is max TPS RPM and max Cμ shown for reference.

Figures 11a and 11b compare variations in C_L and 122° microphone OASPL with Cμ for V = 40 kts, 0° α,for flap angles of 0° and 60°. For both flaps, the OASPL rises quickly with low values of Cμ increasing from 0, then rise less steeply for Cμ > 0.05. The 0° flap OASPL levels off for Cμ > 0.6, while the levels trend higher over the same range for the 60° flap, consistent with the 1/3 octave trends of the Figure 9. Similar OASPL curve trends were observed for the an angle-of-attack of 10° for the 0° flap case (not shown). The red curves in Figs. 11a and 11b indicate the variations in C_L over the range of Cμ. C_L varies from about 0.1 to 1.5 for the 0° flap, and from about 0.5 to 4.05 for the 60° flap. For comparision an aircraft with conventional high-lift system achieves a maximum C_L of about 2.

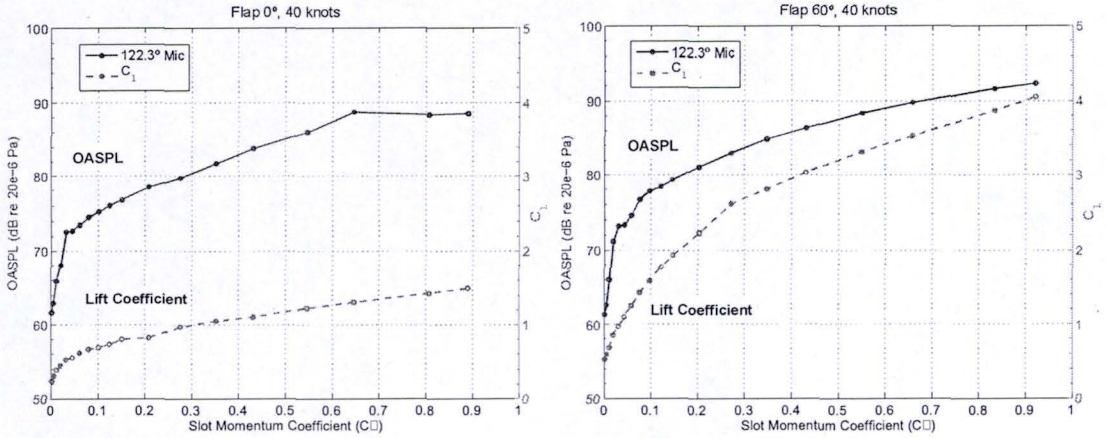

a) 0° flap **b) 60° flap**

Figure 11. Trend of 122° microphone OASPL and lift coefficient with Cμ, V = 40 kts, α = 0°.

For the 40 kt condition, the spectra in Figs. 9a and 9b indicate that the CCW noise is above the fixed-microphone background noise except for the two lowest values of Cμ. The background noise consists sensor in-flow self noise, noise from the support sting and strut, and from the wind tunnel fan drive and other facility sources. These background sources are more prominent at 100 kts, as shown in Fig. 12a for the 122° microphone. At this condition, CCW noise for only the 8 highest values of Cμ are measurably above the background for the fixed microphones. The dark line 20-25 dB below the lowest CCW curve, repeated in the four graphs of Fig. 12, is an effective microphone array processed background noise curve for comparison, described in more detail below.

The microphone array, positioned at a streamwise location comparable to the 122° microphone and located on other side of the model can be used to suppress the three background sources by means of the passive screen, selective region-of-interest beamforming, and with processing methods such as cross-spectral-matrix (CSM) background-noise subtraction as described by Blacodon[10] and implemented in the Optinav software. Fig. 12b shows the array beamform peak level (TIDY process) within the region enclosing the model shown in Figs. 7 and 8. The spectral levels are similar, and background noise is significantly suppressed by 5 dB or more for higher frequencies. With CSM background-noise subtraction, using the Cμ = 0 case as the background measurement, further suppression is demonstrated in Fig. 12c. For comparison, measured background levels for the 122° microphone and array for configurations of sting-only and empty tunnel are shown in Fig. 12d. This demonstration of improved background noise suppression with array processing is the basis for level-sensing array designs such as the SADA array described by Hucheson and Brooks[9], and will be explored further with similar designs in fairings for in-flow measurements.

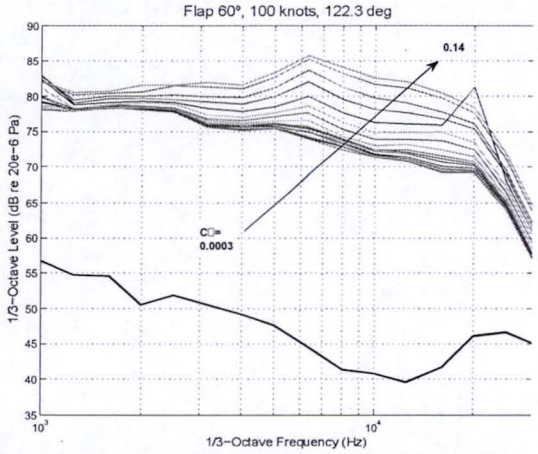

a) **Trend of 122° microphone 1/3-octave spectra variation with momentum coefficient, flap = 60°, α = 0°.**

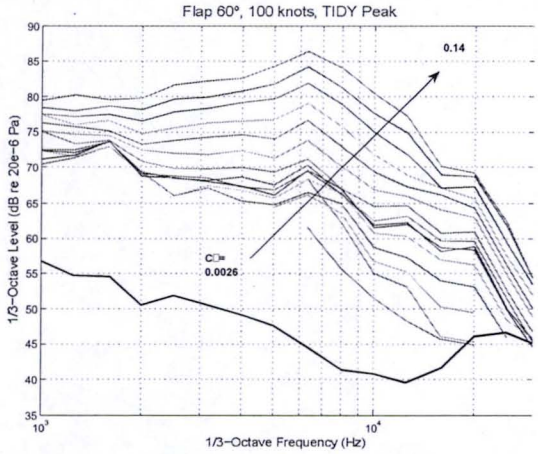

b) **Array peak with TIDY process added to Fig 12a. ROI centered on model.**

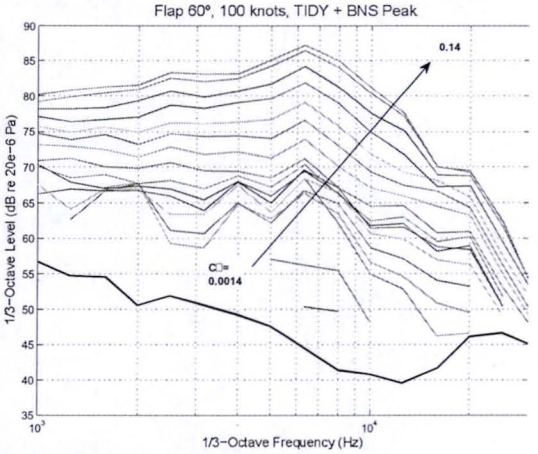

c) **Same processing as Fig. 12b with CSM background-noise subtraction.**

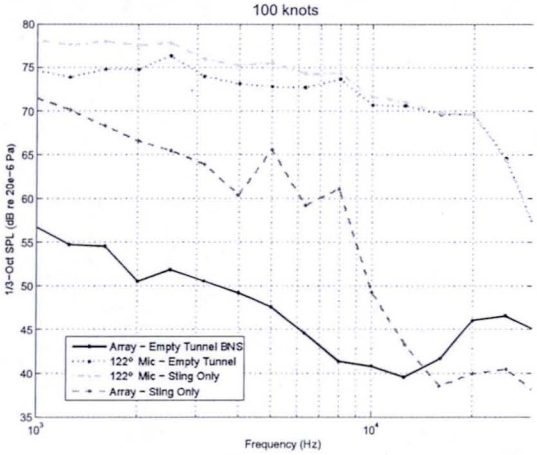

d) **Comparision of single microphone and array background noise.**

Figure 12. Noise source comparison at 100 kts. Dark black curve is the empty tunnel with CSM background-noise subtraction.

V. Summary and Concluding Remarks

Acoustic measurements using fixed microphones and a fixed phased microphone array were taken for nearly all configurations and conditions during a recently concluded wind tunnel test of the AMELIA CESTOL 11% full-span model in the AEDC NFAC 40- by 80-Ft Wind Tunnel. The 10-ft full-span model featured a circulation control wing with inboard and outboard leading- and trailing edge jet slots. Representative data from wind tunnel speeds of 40 and 100 kts, 0° and 60° flap show clear trends in both noise and lift that increase with slot momentum coefficient. Beamform maps of the wing for these conditions show that the slot noise is the dominant field source for most conditions and frequencies when the propulsion simulator was removed. Peak levels from array maps of the region enclosing the model correlated well with fixed microphone spectra from a similar location, and array processing methods including region-of-interest spatial filtering and cross-spectral-matrix background noise subtraction were

effective in significantly reducing the background noise due to the wind tunnel drive, in-flow sensor self-noise, and the unfaired model support system at the higher test speed condition.

Correction of the data for sensor directional response effects is in progress. Release of the full set of corrected data, including propulsion simulator measurements is anticipated next year, with a detailed analysis and report. With the aerodynamic measurements being reported separately. These results will facilite improved simulations of the flight and noise characteristics of active-lift configurations for new models of this class of aircraft.

Appendix

Table 1. CCW slot heights, in thousands of inches.

	Left Wing			Right Wing		
	average	min	max	average	min	max
Leading Edge Inboard	24.46	15.78	30.8	26.43	19.98	32.25
Leading Edge Outboard	24.39	15	36.25	23.44	13.5	35.45
Trailing Edge Inboard	47.05	37.01	53.75	27.81	37.05	56.55
Trailing Edge Outboard	24.53	15.56	46.55	23.68	15.35	37.9

Table 2. Sensor locations (inches) in wind tunnel coordinates referenced to turntable cener. Emission angle and distances are from model center (at 0° α, 0° flap) to sensor.

Sensor	Xw	Yw	Zy	Q	R
Mic 1	-164.9	-247.3	76.4	61.9	336.1
Mic 2	-93.5	-234.8	74.9	75.1	304.9
Mic 3	-40.9	-225.5	74.9	87.1	290.9
Mic 4	4.2	-217.5	74.9	98.5	286.3
Mic 5	49.6	-209.5	74.9	110.0	289.0
Mic 6	101.9	-200.3	74.9	122.3	301.0
Mic 7	174.2	-187.6	74.9	136.3	331.2
Phased Array	90.6	218.2	67.6	119.6	303.2
Acoustic Center (0° α, 0° β)	-29.272	7.154	249.043		

Table 3. CCW mass flow rates and approximate Cμ for sweeps.

total m (lbm/s)	Cμ, 40 kt	Cμ, 100 kt
0	0	0
0.1	0.001	0
0.2	0.005	0
0.3	0.012	0.001
0.4	0.02	0.003
0.5	0.032	0.004
0.6	0.045	0.006
0.7	0.06	0.008
0.8	0.079	0.011
0.9	0.101	0.014
1	0.125	0.018
1.1	0.151	0.021
1.3	0.208	0.03
1.5	0.275	0.041
1.7	0.352	0.053
1.9	0.432	0.066
2.15	0.546	0.085
2.35	0.646	0.102
2.65	0.807	0.129
2.8	0.89	0.144

Acknowledgments

This work was supported by NASA's Fundamental Aeronautics Program Fixed Wing Project.

References

[1] Jameson, K., Marshall, D., Ehrmann, R., Lichward, J., Paciano, E., Burnside, N.J., Fong, R., Horne, W., "Cal Poly's AMELIA 10-Foot Span Hybrid Wing Body Low Noise CESTOL Aircraft Wind Tunnel Test and Experimental Results Overview," 51st AIAA Aerospace Sciences Meeting, Grapevine, TX, January 7-10, 2013.

[2] Burnside, N.J., Horne, W., "Acoustic Surveys of a Scaled-Model CESTOL Transport Aircraft in Static and Forward Speed Conditions," 18th AIAA/CEAS Aeroacoustics Conference, AIAA-2012-2231, Colorado Springs, CO, June 4-6, 2012.

[3] Jameson, K., Marshal, D., Golden, R., Paciano, E., Englar, R., Gaeta, R., Paterson, J, Mason, D., "Part1: The Wind Tunnel Model Design and Fabrication of Cal Poly's AMELIA 10 Foot Span Hybrid Wing-Body Low Noise CESTOL Aircraft," 49th AIAA Aerospace Sciences Meeting, Orlando FL, AIAA-2011-1306, January 4-7, 2011.

[4] Gaeta, R., Englar, R., Avera, M., "Development of Pneumatic Over-the-Wing Powered Lift Technology, Part II: Aeroacoustics," AIAA Applied Aerodynamics Conference, AIAA-2009-3941, San Antonio, TX, June 22-25, 2009.

[5] Dougherty, R., Podboy, G., "Improved Phased Array Imaging of a Model Jet," 15th AIAA/CEAS Aeroacoustics Conference, AIAA-2009-3186, Miami, FL, May 11-13, 2009

[6] Gaeta, R., Lee, W., Flick, A., "Over-the-Wing, Powered Lift, Engine-Airframe Integration Effects on Acoustic Shielding," 47th AIAA Aerospace Sciences Meeting, AIAA-2009-282, Orlando, FL, January 5-8, 2009.

[7] Patterson, G., Joshi, M., Maus, J., "Experimental Investigation of the Aeroacoustic Characteristics of Model Slot Nozzles with Staight Flaps," AIAA 2nd Aeroacoustics Conference, AIAA-75-471, Hampton, VA, March 24-26, 1975.

[8] Crichton, D, *Aeroacoustics of Flight Vehicles Theory and Practice, Vol 1, Noise Sources*, ed. H. Hubbard, Acoustical Society of America, 1995, pp 391-443.

[9] Hutcheson, F., Brooks, T., "Measurement of Trailing Edge Noise Using Directional Array and Coherent Output Power Methods," 8th AIAA/CEAS Aeroacoustics Conference, AIAA-2002-2472, Breckenridge, CO, June 17-19, 2002.

[10] Blacodon, D., "Array Processing for Noisy Data: Aplication for Open and Closed Wind Tunnels," *AIAA Journal*, Vol. 49, No. 1, January 2011.